The Journal of Immunology

The Neurorepellent Slit2 Inhibits Postadhesion Stabilization of Monocytes Tethered to Vascular Endothelial Cells

Ilya Mukovozov, Yi-Wei Huang, Qiuwang Zhang, Guang Ying Liu, Allan Siu, Yaroslav Sokolskyy, Sajedabanu Patel, Sharon J. Hyduk, Michael J. B. Kutryk, Myron I. Cybulsky and Lisa A. Robinson

J Immunol 2015; 195:3334-3344; Prepublished online 21 August 2015;
doi: 10.4049/jimmunol.1500640
http://www.jimmunol.org/content/195/7/3334

The Journal of Immunology is published twice each month by
The American Association of Immunologists, Inc.,
9650 Rockville Pike, Bethesda, MD 20814-3994.

Print ISSN: 0022-1767 Online ISSN: 1550-6606.

The Neurorepellent Slit2 Inhibits Postadhesion Stabilization of Monocytes Tethered to Vascular Endothelial Cells

Ilya Mukovozov,*,† Yi-Wei Huang,* Qiuwang Zhang,‡ Guang Ying Liu,* Allan Siu,§ Yaroslav Sokolskyy,* Sajedabanu Patel,* Sharon J. Hyduk,§ Michael J. B. Kutryk,‡ Myron I. Cybulsky,§ and Lisa A. Robinson*,†

The secreted neurorepellent Slit2, acting through its transmembrane receptor, Roundabout (Robo)-1, inhibits chemotaxis of varied cell types, including leukocytes, endothelial cells, and vascular smooth muscle cells, toward diverse attractants. The role of Slit2 in regulating the steps involved in recruitment of monocytes in vascular inflammation is not well understood. In this study, we showed that Slit2 inhibited adhesion of monocytic cells to activated human endothelial cells, as well as to immobilized ICAM-1 and VCAM-1. Microfluidic live cell imaging showed that Slit2 inhibited the ability of monocytes tethered to endothelial cells to stabilize their actin-associated anchors and to resist detachment in response to increasing shear forces. Transfection of constitutively active plasmids revealed that Slit2 inhibited postadhesion stabilization of monocytes on endothelial cells by preventing activation of Rac1. We further found that Slit2 inhibited chemotaxis of monocytes toward CXCL12 and CCL2. To determine whether Slit2 and Robo-1 modulate pathologic monocyte recruitment associated with vascular inflammation and cardiovascular disease, we tested PBMC from patients with coronary artery disease. PBMC from these patients had reduced surface levels of Robo-1 compared with healthy age- and sex-matched subjects, and Slit2 failed to inhibit chemotaxis of PBMC of affected patients, but not healthy control subjects, toward CCL2. Furthermore, administration of Slit2 to atherosclerosis-prone LDL receptor–deficient mice inhibited monocyte recruitment to nascent atherosclerotic lesions. These results demonstrate that Slit2 inhibits chemotaxis of monocytes, as well as their ability to stabilize adhesions and resist detachment forces. Slit2 may represent a powerful new tool to inhibit pathologic monocyte recruitment in vascular inflammation and atherosclerosis. ***The Journal of Immunology*****, 2015, 195: 3334–3344.**

Vascular inflammation associated with cardiovascular disease is the leading cause of morbidity and mortality in the Western world (1, 2). At the center of this disease process is recruitment of circulating monocytes into the injured vascular wall. In human subjects, polymorphisms in the chemokine receptors CCR2 and CX_3CR1, which result in reduced chemotaxis of monocytes, are highly protective against adverse cardiovascular events (3, 4). Mice deficient in CCR2, CX_3CR1, and CCR5 demonstrate decreased monocyte trafficking into vascular lesions, and combined blockade of all three confers additive protection (5–9). Once recruited, monocytes adhere to inflamed endothelium before traversing into the subendothelial space (2, 10). This requires tethered monocytes to resist detachment caused by forces transmitted by flowing blood. Stabilization of monocyte anchors is dependent on actin cytoskeletal rearrangements and activation of Rac (11). Thus, a strategy to simultaneously block chemotaxis of monocytes to different attractants, as well as postadhesion stabilization of monocytes tethered to inflamed endothelium, could prove highly effective in preventing vascular inflammation. A means to achieving this can be exploited from neuronal guidance cues that direct cell migration during development.

The Slit family of secreted proteins, acting through their transmembrane receptor Roundabout (Robo), repels migrating neurons during development (12, 13). Slit and Robo are also expressed in mature organisms, and an isoform of Robo, Robo-1, was detected on the surface of cells involved in vascular injury, including neutrophils, vascular smooth muscle cells (VSMC), lymphocytes, and monocytes (14–19). In neuronal cells, Slit2 promotes recruitment of soluble Slit Robo GTPase-activating protein to the cytoplasmic tail of Robo-1, in turn preventing activation of the Rho family GTPases Rac and Cdc42 (20). We (17, 21) and other investigators (14–16, 18, 19) showed that secreted Slit2 interacts with Robo-1 on the surface of human PBMC, neutrophils, VSMC, and monocytes to inhibit migration of these cells toward diverse inflammatory chemoattractant cues both in vitro and in vivo. We observed that binding of Slit2 to Robo-1 prevented activation of Cdc42 and Rac, thereby preventing the actin polymerization and cell polarization necessary for directional migration of leukocytes (17). However, the precise effects of Slit2 on the steps that govern monocyte recruitment in vascular inflammation are not well understood (21).

In this article, we report that primary human and murine monocytes express the Slit2 receptor, Robo-1 and that Slit2 inhibits not only monocyte chemotaxis but also the stabilization of adhesion of monocytes tethered to endothelial cells. We further report that

*Program in Cell Biology, The Hospital for Sick Children Research Institute, Toronto, Ontario M5G 1X8, Canada; †Institute of Medical Science, University of Toronto, Toronto, Ontario M5S 1A8, Canada; ‡Division of Cardiology, Keenan Research Center for Biomedical Science, Li Ka Shing Knowledge Institute, St. Michael's Hospital, Toronto, Ontario M5B 1T8, Canada; and §Toronto General Research Institute, University Health Network, Toronto, Ontario M5G 2C4, Canada

Received for publication March 16, 2015. Accepted for publication July 22, 2015.

This work was supported by the Canadian Institutes of Health Research (Grant MOP-111083 to L.A.R.).

Address correspondence and reprint requests to Dr. Lisa A. Robinson, The Hospital for Sick Children, 555 University Avenue, Room 5265, Toronto, ON M5G 1X8, Canada. E-mail address: lisa.robinson@sickkids.ca

The online version of this article contains supplemental material.

Abbreviations used in this article: CAD, coronary artery disease; CA-Rac1-GFP, constitutively-active Rac1-GFP; HAEC, human aortic endothelial cell; LatB, latrunculin B; Robo, Roundabout; VSMC, vascular smooth muscle cell; WT-Rac1-GFP, wild-type Rac1-GFP.

PBMC from patients with coronary artery disease (CAD) have decreased expression of Robo-1, resulting in decreased responsiveness to the actions of Slit2. Using atherosclerosis-prone LDL receptor-deficient ($Ldlr^{-/-}$) mice, we found that administration of Slit2 inhibited early monocyte recruitment to nascent vascular lesions. Together, these data support a role for Slit2 in preventing early vascular inflammation.

Materials and Methods

Reagents and Abs

Unless otherwise stated, reagents were purchased from Sigma-Aldrich (St. Louis, MO). Monocyte isolation kits were purchased from STEMCELL Technologies (Vancouver, BC, Canada). Anti-human Robo-1 Ab was from Rockland Immunochemicals (Gilbertsville, PA). Anti-Cdc42, anti-Rac1, anti-Erk, anti–phospho-Erk, anti-Akt, and anti–phospho-Akt Abs were from Cell Signaling (Danvers, MA). Alexa Fluor–conjugated Ab, Hoechst 33342, and BrdU were from Invitrogen (Burlington, ON, Canada). Anti-CD45 Ab was purchased from eBioscience (San Diego, CA). Allophycocyanin anti-mouse Ly6C Ab and biotin anti-mouse CD115 were purchased from BioLegend (San Diego, CA). HRP-conjugated and DyLight-conjugated Ab, Cy3-conjugated anti-rabbit IgG, Cy2-conjugated anti-human IgG, and HRP-conjugated anti-rabbit IgG were purchased from Jackson ImmunoResearch Laboratories (West Grove, PA). VCAM-1/Fc and ICAM-1/Fc chimeric proteins were purchased from R&D Systems (Minneapolis, MN). CCL2 and CXCL12 were purchased from PeproTech (Rocky Hill, NJ). FITC-conjugated anti-BrdU, anti–β-actin, and HRP-conjugated anti-FITC Ab were from Abcam (Cambridge, MA). FITC-tyramide was purchased from PerkinElmer (Cambridge, MA). mAb24, which recognizes functionally active β2 integrins molecules, was purchased from Hycult Biotech (Plymouth Meeting, PA).

Cell culture

THP-1 and U937 human monocytic cells (American Type Culture Collection) were cultured in RPMI 1640 (Sigma-Aldrich) containing 10% FBS. HUVEC and human aortic endothelial cells (HAEC; Lonza, Walkersville, MD) were grown in Endothelial Basal Medium-2 containing Clonetics EGM-2 SingleQuots (Lonza). Only cells from passages four through eight were used.

Expression plasmids encoding wild-type GFP-tagged Rac1 (WT-Rac1-GFP) and a constitutively active allele of Rac1 (CA-Rac1-GFP) were kind gifts from Dr. Sergio Grinstein (The Hospital for Sick Children) (22). U937 cells were electroporated with the plasmids using the Cell Line Nucleofector Kit V (Lonza) and the Nucleofector II program V-001. FACS was performed using an Astrios MoFlo (Beckman Coulter) to isolate GFP^+ cells.

Isolation of human and mouse monocytes and PBMC

Monocytes were isolated from the blood of healthy volunteers using Polymorphprep gradient separation solution (Axis-Shield, Oslo, Norway) and an EasySep Negative Selection Kit (STEMCELL Technologies) (11). Cell viability was determined to be >98% by trypan blue staining. Mouse blood was obtained by cardiac puncture, and monocytes were isolated using an EasySep Mouse Monocyte Enrichment Kit (STEMCELL Technologies). In some experiments, PBMC were isolated from the blood of patients with CAD or from healthy age- and sex-matched controls by Ficoll gradient centrifugation (11). Informed consent for study participation was obtained from all patients and healthy volunteers. All protocols involving human samples were approved by the Research Ethics Board of St. Michael's Hospital in accordance with The Code of Ethics of the World Medical Association (Declaration of Helsinki). Patients with stable CAD, who were scheduled to undergo percutaneous coronary intervention, were recruited. A total of 10 patients and 8 age- and gender-matched healthy subjects was recruited.

Expression and purification of Slit2, N-Slit2, Slit2ΔD2, C-Slit2, and RoboN

Full-length Slit2 and bioactive truncated N-Slit2 were purified as previously described (17, 21, 23). N-Slit2 was also purchased from PeproTech. Slit2ΔD2, a Slit2 mutant that lacks the D2 domain required to bind Robo-1, and RoboN, the soluble N-terminal region comprising aa 60–870 of Robo-1, were purified as previously described (21). C-Slit2, an inactive fragment comprising aa 1268–1525 of Slit2, was cloned in pTT28 using BamHI restriction sites and purified as described for N-Slit2, RoboN, and Slit2ΔD2 (17, 21, 24).

RNA extraction and RT-PCR

Total RNA was extracted from PBMC using a miRNeasy Mini Kit (QIAGEN, Toronto, ON, Canada), according to the manufacturer's instructions. The first-strand cDNA was generated by reverse transcription using an Omniscript RT Kit (QIAGEN). Robo-1 was semiquantified using VisionWorksLS Image Acquisition and Analysis Software (UVP Bioimaging Systems, Upland, CA), with GAPDH used as an internal control. Primers for each gene amplification were designed to span an intron to eliminate detection of genomic contamination. The following primer sequences were used: human Robo-1 (GenBank gene accession number NM_002941.3), sense 5′-GCTGTGAGCCACAATGCATCGCTG-3′ and antisense 5′-GTGATCATGAGCTTTCCTCCT-3′; and GAPDH (gene accession number: x02231), sense 5′-CTCTAAGGCTGTGGGCAAGGTCAT-3′ and antisense 5′-GAGATCCACCACCCTGTTGCTGTA-3′.

Immunofluorescence microscopy

Primary human and murine monocytes, as well as cultured THP-1 cells and U937 cells, were allowed to adhere to fibronectin- or poly-L-lysine–coated coverslips. Cells were fixed with 4% paraformaldehyde, incubated with rabbit anti–Robo-1 Ab (1 μg/ml) for 2 h, washed, and then incubated with Cy3-conjugated anti-rabbit IgG and Alexa Fluor 488–conjugated wheat germ agglutinin to visualize the plasma membrane. A Leica DMIRE2 spinning disc confocal microscope (Leica Microsystems, Toronto, ON, Canada) equipped with a Hamamatsu back-thinned EM-CCD camera and Volocity software (Improvision, Lexington, MA) was used to capture images.

Cell migration assays

Transwell migration assays were performed as previously described (17). Monocytic cells were incubated with control vehicle or with Slit2 (0.3–30 nM) placed in the upper well of the Transwell chamber, and CXCL12 (100 ng/ml) or CCL2 (20 ng/ml) was placed in the lower well. Cell migration into the lower well was examined after 3 h (17).

In some experiments, a FluoroBlok 24-well Insert System (pore size 5 μm; BD Biosciences, Oakville, ON, Canada) was used to perform modified Boyden chamber migration assays. PBMC were labeled with Calcein, AM (Life Technologies, Burlington, ON, Canada) and washed three times. PBMC (1×10^6) were incubated with recombinant Slit2 protein (4 nM) at 37°C for 10 min and then transferred to the top chamber. CCL2 (50 ng/ml) or control medium was placed in the bottom well. After 1 h, PBMC migration was assessed by measuring the fluorescence intensity in the bottom chamber using a fluorescence reader, with excitation set at 490 nm and emission at 530 nm. The percentage of cell migration in the presence of Slit2 over cell migration in the absence of Slit2 was used to express the inhibitory effect of Slit2 on PBMC migration.

Adhesion assays

Primary HUVEC and HAEC were grown to confluence and incubated with TNF-α (20 ng/ml) for 4 h. THP-1 cells were labeled with Calcein, AM, and adhesion assays were performed as described (23). Nonadherent monocytic cells were removed by centrifuging the plates ($100 \times g$, 1 min) upside down (23). A fluorescent plate reader was used to measure the fluorescence intensity of each well. Fluorescence intensity was normalized to the corresponding unstimulated condition. In some experiments, adhesion of monocytic cells to immobilized ICAM-1 and VCAM-1 was examined, as described above (25).

Murine peritonitis experiments

Murine peritonitis experiments were carried out as previously described (17, 26). All procedures were performed in accordance with the *Guide for the Humane Use and Care of Laboratory Animals* and were approved by The Hospital for Sick Children Research Institute Animal Care Committee. Slit2 (2 μg) was administered i.p. or i.v. via tail vein injection to BALB/c and CD1 mice (Charles River Canada, Saint-Constant, QC, Canada) 1 h prior to i.p. injection of sodium periodate (1 mg) (17). Peritoneal lavage was performed after 24 h; cells were recovered, washed, and counted using a hemocytometer after lysis of contaminating RBCs. In some experiments, peritoneal cells were fixed, labeled with anti-mouse F4/80 Ab, and analyzed by flow cytometry. More than 75% of peritoneal cells recovered were positive for F4/80, consistent with a macrophage phenotype (data not shown).

Immunoblotting

Immunoblotting was performed as previously described (17, 21). THP-1 cells were serum starved overnight and then incubated with either PBS

vehicle or Slit2 (30 nM) for 10 min and then with PBS vehicle or CXCL12 (100 ng/ml) for 2 min (17, 21). All samples were pipetted in the same manner. Protein lysate was extracted, and immunoblotting was performed using Ab directed to phospho-Akt or phospho-Erk. Blots were stripped and reprobed with Ab detecting total Akt and Erk (17, 21). ImageJ software (National Institutes of Health, Bethesda, MA) was used for densitometry analysis. In some experiments, lysates were obtained from PBMC, as well as from human and murine monocytes, and immunoblotting was performed using an Ab to detect Robo-1.

Cdc42- and Rac1-activation assays

Immunoprecipitation and immunoblotting experiments were performed as previously described, using the p21-binding domain (aa 67–150) of p21/Cdc42/Rac1-activated kinase 1 (17, 21). THP-1 cells were incubated with Slit2 (30 nM) for 10 min and then with CXCL12 (100 ng/ml) for 0 or 2 min. In some experiments, U937 cells were allowed to adhere to HUVEC monolayers that had been activated with TNF-α and fixed with 4% paraformaldehyde. Active Rac1 was detected as described previously (17, 21).

Flow cytometry

THP-1 cells, U937 cells, and primary human and murine monocytes were incubated with Ab detecting Robo-1, followed by PE-conjugated secondary Ab, and flow cytometry was performed as previously described (17, 21). To quantify activation of β1 integrins on the surface of U937 cells, binding of FITC-conjugated peptide 4-((N′-2-methylphenyl)ureido)-phenylacetyl-*l*-leucyl-*l*-α-aspartyl-*l*-valyl- *l*-prolyl-*l*-alanyl-*l*-alanyl-*l*-lysine was assessed by flow cytometry as previously described (25). Cells were treated with N-Slit2 (30 nM) for 10 min and then incubated with CXCL12 (100 ng/ml) for 0 or 2 min. Activation of β2 integrins was determined using the (CD11/CD18) β2 integrin activation reporter Ab mAb24 (Hycult Biotech), which only binds active β2 integrins (27).

BioFlux microfluidics assays

Confluent HUVEC monolayers were grown in fibronectin-coated BioFlux microfluidic channels (Fluxion Biosciences, San Francisco, CA) and incubated with TNF-α for 4 h (23). Monocyte- accumulation and -detachment assays were performed as previously described (11, 23). Leukocytes were incubated with Slit2 (30 nM), latrunculin B (LatB; 2 μM), or control vehicle.

Accumulation assays. Monocytic cells (5.0×10^6 cells/ml) were infused in microfluidic channels at a wall shear stress of 2 dyn/cm^2. The number of leukocytes that interacted with the monolayer or that remained stationary for >2 s was determined in real time using images from 30× fields (23).

Detachment assays. Monocytic cells were infused in the microfluidic channels and allowed to settle under static conditions onto the endothelial monolayers for 1 min. After static adhesion, shear force was introduced and incrementally increased by 1 dyn/cm^2 at 10-s intervals from 1 to 10 dyn/cm^2 and then increased incrementally by 5 dyn/cm^2. The number of cells remaining adherent after each interval was determined using BioFlux acquisition software (11).

Assessment of monocyte recruitment in Ldlr$^{-/-}$ *mice*

Ldlr$^{-/-}$ mice, backcrossed for >10 generations onto the C57BL/6 background, were obtained from The Jackson Laboratory. All procedures were approved by the University Health Network Animal Care Committee. At 10–12 wk of age, *Ldlr*$^{-/-}$ mice were switched to a 1.25% cholesterol-rich diet and maintained on this diet for 3 wk (28). Mice received a single i.v. injection of BrdU (2 mg) in PBS. Three hours following BrdU injection, an i.v. injection of N-Slit2 (5 μg) or PBS vehicle was administered.

Aortas were harvested 3 or 24 h after BrdU injection (29). Following perfusion fixation (4% paraformaldehyde, 100 mm Hg), careful dissection of the surrounding adipose tissue was performed (29). For detection of BrdU-labeled intimal cells, aortas were permeabilized (0.5% Triton X-100 for 15 min) and incubated sequentially with 0.3% H_2O_2 (30 min), 1 M HCl (1 h at 37°C), FITC-conjugated anti-BrdU (2 μg/ml; 18 h at 4°C), HRP-conjugated anti-FITC (3 μg/ml), and FITC-tyramide (29). Lipid accumulated in lesions was detected by Nile Red staining, and nuclei were counterstained with Hoechst 33342 (2 μg/ml) (29). Anti-CD45 Ab (eBioscience) was used to label infiltrating leukocytes. A confocal microscope (FV-1000; Olympus) with a 40× (NA 1.3) oil-immersion objective was used to acquire images.

Statistical analysis

ANOVA followed by the Tukey post hoc test were performed using GraphPad Prism statistical software to analyze the data from experiments with multiple comparisons. In all other cases, the Student *t* test was used. A significant difference was considered at $p < 0.05$. Data represent mean ± SEM.

Results

Human and murine monocytes express the Slit2 receptor Robo-1

Using immunoblotting, immunofluorescence microscopy, and flow cytometry, Robo-1 protein was detected in cultured human monocytic cells and primary human and mouse monocytes (Fig. 1). Robo-2 and -4 were not detected in the monocytic cell types studied (data not shown).

Slit2 inhibits monocyte chemotaxis to diverse chemokines

To study the effects of Slit2 on the migration of monocytic cells, we performed Transwell chemotaxis assays (30). Basal migration was negligible (Fig. 2A, 2F) but increased significantly toward a gradient of the chemokine CCL2 (Fig. 2B, 2F, $p < 0.001$). Slit2 inhibited cell chemotaxis in a concentration-dependent manner (Fig. 2A–F, $p < 0.001$ for CCL2 versus 30 nM Slit2; $p < 0.05$ for CCL2 versus 3 nM Slit2 and for 30 nM Slit2 versus 0.3 nM Slit2). To determine whether Slit2 inhibits monocytic cell migration toward chemokines belonging to different classes, we performed Transwell assays using CXCL12. Migration increased significantly toward a gradient of CXCL12 (Fig. 2G, $p < 0.001$) and was inhibited by Slit2 (Fig. 2G, $p < 0.05$). To confirm the specificity of the observed inhibition, we tested a bioactive N-terminal fragment of Slit2 (N-Slit2), containing the leucine-rich regions required to bind Robo-1 (31). N-Slit2 also significantly inhibited monocytic cell chemotaxis (Fig. 2G, $p < 0.05$).

We also performed Transwell assays using primary human monocytes and U937 monocytic cells and, in both instances, N-Slit2 significantly inhibited cell migration toward the chemokine CXCL12 (Fig. 2H, 2I, primary monocytes, $p < 0.001$; U937, $p < 0.05$). To confirm that the observed effects of Slit2 did not result from nonspecific protein binding, we used a Slit2 mutant Slit2ΔD2 (21, 23). As expected, Slit2ΔD2 did not inhibit monocytic cell migration toward CXCL12 (Fig. 2I, $p < 0.01$, versus N-Slit2). Similarly, C-Slit2 did not inhibit chemotaxis (Fig. 2I, $p < 0.05$, versus N-Slit2) (21, 23). To verify the specificity of the observed Slit2-induced effects, we used RoboN, a soluble truncated version of the Robo-1 receptor that acts as a decoy receptor for Slit2, preventing its binding to cell surface Robo-1 receptors (18, 23). Preincubation of N-Slit2 with RoboN abolished the inhibitory effect of N-Slit2 (Fig. 2I, $p < 0.01$, versus N-Slit2), providing further support that the inhibitory effects of Slit2 are Robo-1 dependent. These data demonstrate that Slit2 is a potent inhibitor of monocytic cell chemotaxis toward different classes of chemokines.

Slit2 inhibits chemokine-induced activation of Rac1 and Cdc42

Chemotactic stimulation of monocytes results in activation of the Rho family GTPases, Rac and Cdc42 (32, 33). Because the predominant isoform of Rac in human monocytes is Rac1, we specifically examined the activation of Rac1 (34). Unstimulated THP-1 cells had low basal levels of activated Rac1 and Cdc42 (Fig. 3A–D). Exposure to CXCL12 increased levels of activated Rac1 by >20-fold (Fig. 3A, 3B, $p < 0.001$) and the levels of activated Cdc42 by 5-fold (Fig. 3C, 3D, $p < 0.001$). Slit2 did not affect basal levels of activated Rac1 and Cdc42, but it inhibited CXCL12-induced activation of Rac1 (Fig. 3A, 3B, $p < 0.05$) and Cdc42 (Fig. 3C, 3D, $p < 0.05$). These data demonstrate that Slit2 inhibits monocytic cell chemotaxis by preventing activation of Rac1 and Cdc42.

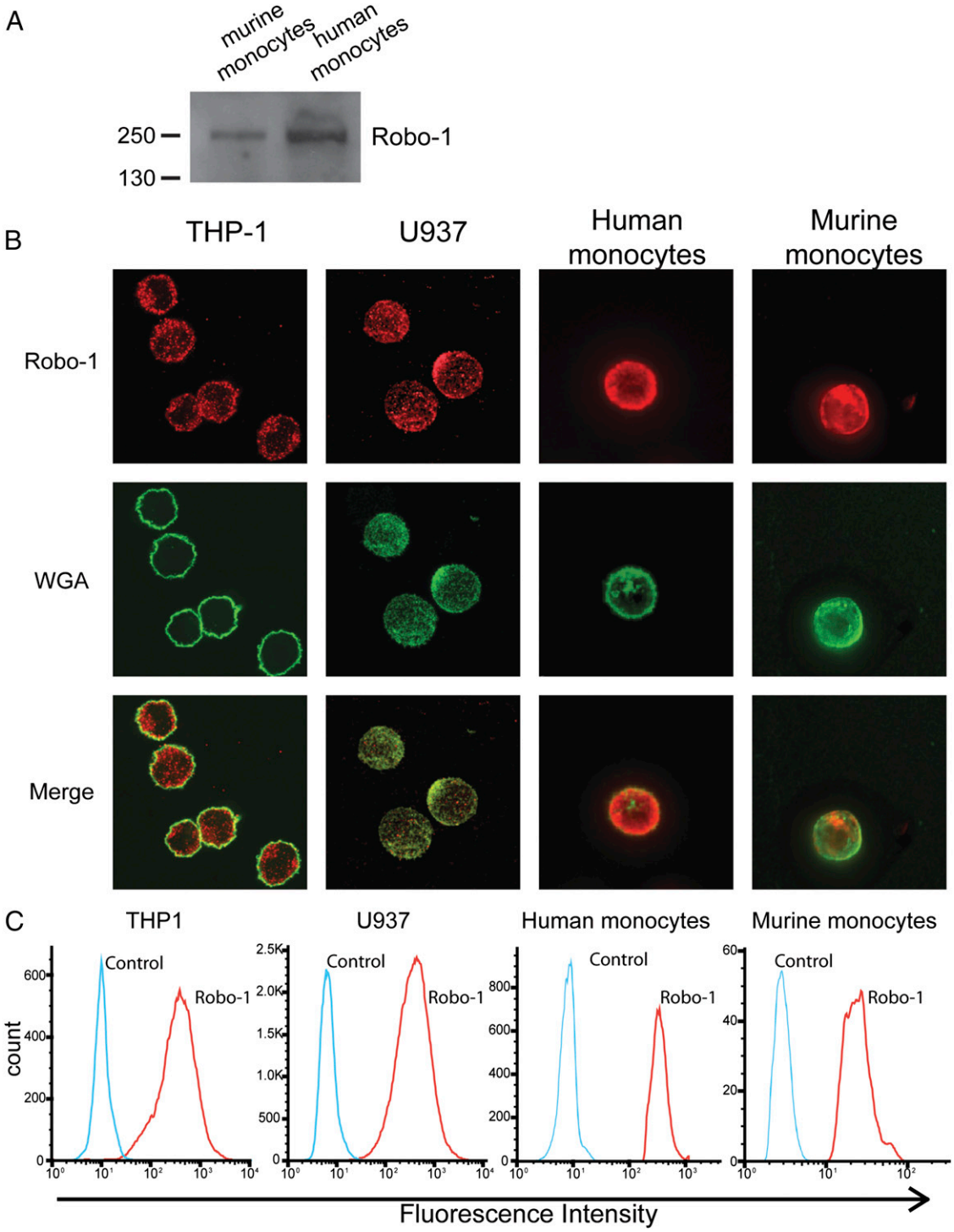

FIGURE 1. Human and mouse monocytes express Robo-1. (**A**) Cell lysates from primary human monocytes and bone marrow–derived murine monocytes were harvested, and immunoblotting was performed using anti–Robo-1 primary Ab and HRP-conjugated secondary Ab. (**B**) THP-1 cells, U937 cells, primary human monocytes, and primary murine monocytes on fibronectin- or poly-L-lysine–coated coverslips were labeled with anti–Robo-1 Ab, followed by Cy3-conjugated secondary Ab and Alexa Fluor 488–conjugated wheat germ agglutinin (WGA). Cells were examined using a Leica DMIRE2 spinning disc confocal microscope (original magnification ×150). (**C**) Human monocytes were isolated as in (A). Cells from murine blood were labeled with anti-Ly6C allophycocyanin Ab, biotin anti-CD115 Ab, and streptavidin–Alexa Fluor 488. Cells were fixed, incubated with anti–Robo-1 Ab, followed by PE-conjugated secondary Ab or with secondary Ab alone, and analyzed by flow cytometry. Cells were gated based on forward scatter area and side scatter area. For murine monocytes, Robo-1 expression is shown for $Ly6C^{high}$ and $CD115^{+}$ cells. Representative images from one of three similar independent experiments.

Slit2 inhibits chemokine-induced activation of PI3K and Erk1/2

We studied the effects of Slit2 on the activation of kinase signaling pathways known to be associated with monocyte chemotaxis: PI3K/Akt, and Erk (11, 35). Stimulation with CXCL12 induced robust phosphorylation of Akt (Fig. 3E, 3F, $p < 0.01$) and Erk (Fig. 3G, 3H, $p < 0.001$). Incubation with Slit2 alone had no effect on basal levels of kinase activation (Fig. 3E–H). However, Slit2 significantly inhibited CXCL12-mediated phosphorylation of Akt

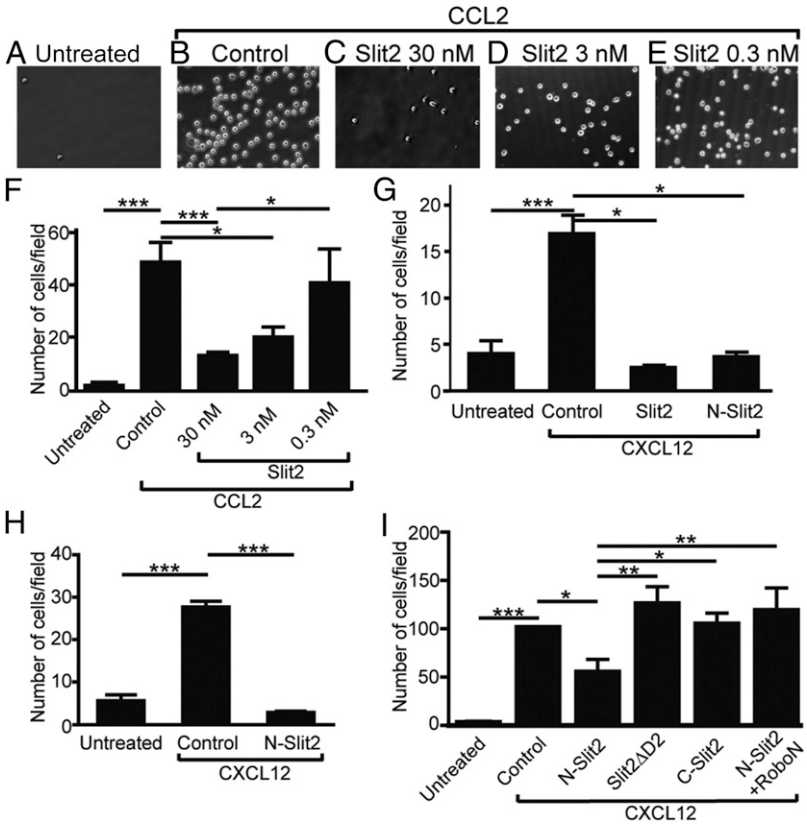

FIGURE 2. Slit2 inhibits monocyte chemotaxis to different chemokines. (**A**–**E**) THP-1 cells were incubated with Slit2 at the indicated concentrations for 10 min at 37°C, and migration assays were performed across 5-μm Transwell inserts. The lower chamber contained RPMI 1640 or Slit2-containing RPMI 1640 in the presence or absence of CCL2 (20 ng/ml). Cells were placed in the upper chamber, and plates were incubated for 3 h at 37°C. The insert was removed, cells that had migrated to the lower chamber were centrifuged gently onto coverslips, and cell nuclei were labeled with DAPI. Representative high-power images (original magnification ×60) from 10 independent experiments were taken using a Leica deconvolution microscope. (A) Control vehicle. (B) CCL2. (C) Slit2 (30 nM) and CCL2. (D) Slit2 (3 nM) and CCL2. (E) Slit2 (0.3 nM) and CCL2. (**F**) Assays were performed as above in the presence of the indicated concentrations of Slit2. At least 10 random fields were counted. Data are mean ± SEM from 10 independent experiments. (**G**) Transwell migration assays were performed as above. CXCL12 (100 ng/ml) was placed in the lower chamber in the presence or absence of purified Slit2 (30 nM) or N-Slit2 (30 nM). Data are mean ± SEM from four independent experiments. (**H**) Experiments were performed as in (G) using primary human monocytes. CXCL12 (100 ng/ml) was placed in the lower chamber in the presence or absence of purified N-Slit2 (30 nM). Data are mean ± SEM from five independent experiments. (**I**) Experiments were performed as in (G) using U937 cells. CXCL12 (100 ng/ml) was placed in the lower chamber in the presence or absence of purified N-Slit2 (30 nM), Slit2ΔD2 (30 nM), C-Slit2 (30 nM), or N-Slit2 (30 nM) + RoboN (60 nM). Data are mean ± SEM from 11 independent experiments. $*p < 0.05$, $**p < 0.01$, $***p < 0.001$.

(Fig. 3E, 3F, $p < 0.05$) and Erk (Fig. 3G, 3H, $p < 0.01$). These data suggest that Slit2 inhibits chemokine-induced activation of Akt and Erk signaling in monocytic cells.

Slit2 inhibits adhesion of monocytes to activated endothelial cells and to immobilized VCAM-1 and ICAM-1

We showed that Slit2 prevents activation of Cdc42, Rac1, PI3K/Akt, and Erk, which mediate multiple steps of the adhesion cascade, culminating in firm arrest of monocytes under shear flow (25, 35). We next investigated the effects of Slit2 on the adhesion of monocytic cells to endothelial cell monolayers. TNF-α significantly increased adhesion to venous and arterial endothelial cells (Fig. 4A, 4B, $p < 0.01$), and incubation of monocytic cells with N-Slit2 significantly diminished adhesion (Fig. 4A, 4B, $p < 0.05$). To selectively study Slit2's effects on monocytic rather than endothelial cells, we examined monocytic cell adhesion to immobilized adhesion ligands (25). Cell adhesion to ICAM-1– and VCAM-1–coated surfaces was significantly greater relative to BSA (Fig. 4C, 4D, $p < 0.05$, ICAM-1 versus 1% BSA; $p < 0.001$, VCAM-1 versus 1% BSA), and N-Slit2 significantly decreased adhesion to ICAM-1 and VCAM-1 (Fig. 4C, 4D, $p < 0.05$). These data demonstrate that Slit2 acts on monocytes to inhibit their adhesion to ICAM-1 and VCAM-1, which are abundantly expressed on the surface of activated endothelial cells (Supplemental Fig. 1).

Slit2 inhibits recruitment of monocytes/macrophages in vivo

To study the effects of Slit2 on recruitment of monocytes/macrophages in vivo, we used a mouse model of chemical irritant peritonitis (17, 26). Sodium periodate induced recruitment of monocytes/macrophages into the peritoneal cavity (Fig. 5A, $p < 0.001$), and i.p. administration of Slit2 1 h prior to induction of peritonitis inhibited leukocyte influx (Fig. 5A, $p < 0.001$). Slit2 administered i.v. 1 h prior to induction of peritonitis also blunted monocyte/macrophage accumulation in the peritoneum after 24 h (Fig. 5B, $p < 0.05$). These results are in keeping with our previous observation that Slit2 blocked neutrophil recruitment to the peritoneum following induction of peritonitis (17). Slit2 retained its biological activity, even when administered up to 4 d before induction of peritonitis (Fig. 5C, 1 d, $p < 0.001$; 4 d, $p < 0.01$). To ensure that Slit2 did not deplete circulating monocytes, we measured monocyte levels in murine blood 1 and 4 d after administration of Slit2. No difference in the number of circulating monocytes was observed (Fig. 5D). More than 75% of peritoneal cells recovered were positive for F4/80, consistent with a monocyte/macrophage phenotype (data not shown).

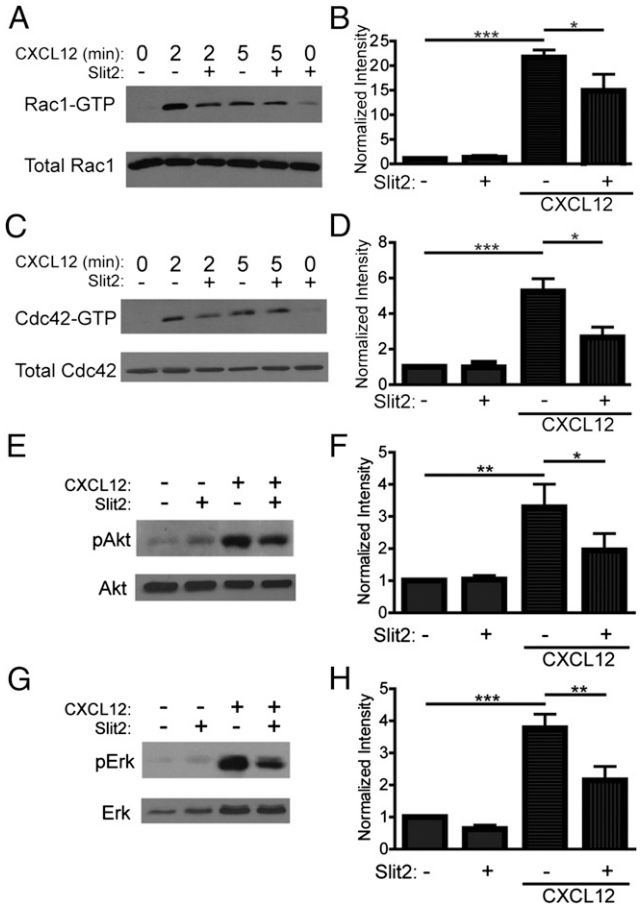

FIGURE 3. Slit2 inhibits CXCL12-mediated activation of Cdc42, Rac1, PI3K/Akt, and Erk1/2 in monocytic cells. (**A**) THP-1 cells were incubated with PBS or CXCL12 (100 ng/ml for 2 or 5 min) in the presence or absence of Slit2, and cell lysates were collected. GST beads conjugated to the PBD of PAK1 were used to pull down activated Rac, and immunoblotting was performed using a specific Ab directed against Rac1. Representative blot from one of four independent experiments. (**B**) Experiments were performed as in (A). Data are mean ± SEM of normalized band intensities. (**C**) Experiments were performed as in (A), using Ab directed against Cdc42. (**D**) Experiments were performed as in (C). Data are mean ± SEM from four independent experiments. (**E**) THP-1 cells were incubated with PBS or CXCL12 (100 ng/ml for 2 min) in the presence or absence of Slit2, and cell lysates were collected. Immunoblotting was performed using Ab detecting p-Akt. Blots were stripped and reprobed using Ab detecting total Akt. Representative blot from one of seven experiments. (**F**) Experiments were performed as in (E). Band intensities for p-Akt normalized to total Akt. Data are mean ± SEM. (**G**) Experiments were performed as in (E), using Ab detecting p-Erk and total Erk. (**H**) Experiments were performed as in (G). Band intensities for p-Erk normalized to total Erk. Data are mean ± SEM for six independent experiments. $*p < 0.05$, $**p < 0.01$, $***p < 0.001$.

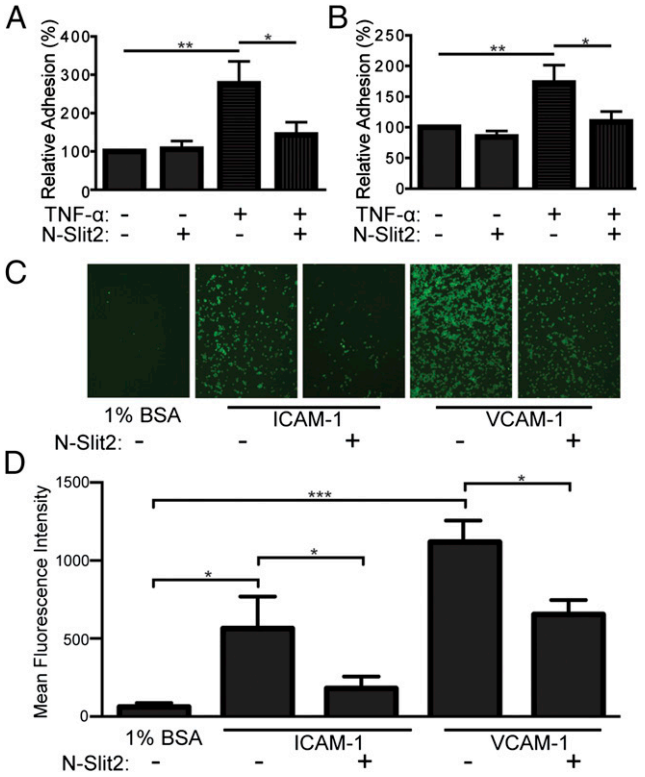

FIGURE 4. Slit2 inhibits adhesion of monocytic cells to endothelial cells and to immobilized ICAM-1 and VCAM-1. (**A**) THP-1 cells were labeled with Calcein, AM, incubated with N-Slit2 or control vehicle for 10 min, and allowed to adhere to HUVEC monolayers exposed to TNF-α for 4 h. After 30 min, nonadherent THP-1 cells were removed by centrifuging the plates upside down at 100 × *g*, and a fluorescent plate reader was used to quantify adherent cells. Data are mean ± SEM from five independent experiments. (**B**) Experiments were performed as in (A) using TNF-α–activated HAEC instead of HUVEC. Data are mean ± SEM from eight independent experiments. (**C**) Experiments were performed as in (A), using wells coated with 1% BSA, ICAM-1/Fc, or VCAM-1/Fc instead of HUVEC. Wells were imaged using a Leica deconvolution microscope (original magnification ×15). Representative images from 1 of 11 independent experiments. (**D**) Experiments were performed as in (C), and adhesion was quantified as in (A). Data are mean ± SEM from 11 independent experiments. $*p < 0.05$, $**p < 0.01$, $***p < 0.001$.

Slit2 does not inhibit monocyte tethering, rolling, or accumulation under shear flow

We found that Rac1 is robustly activated in monocytes during adhesion to endothelial cells (Supplemental Fig. 2). Therefore, we tested the effects of Slit2 on adhesion of monocytes exposed to shear flow, where Rac1 activation is critical for cells to maintain stable adhesions and resist detachment (11).

Using a microfluidic system to mimic shear-regulated integrin activation encountered in the vasculature, we found that, at 2 dyn/cm^2, exposure to N-Slit2 did not affect monocyte capture, rolling, or firm arrest on TNF-α–activated endothelial cell monolayers (Fig. 6A–C) (21, 23). Because selectin-mediated signaling can slow down rolling or tethering cells, we calculated the rolling velocity and observed that N-Slit2 did not change the average rolling velocity of cells (Fig. 6D). Furthermore, exposure to N-Slit2 did not prevent chemokine-induced activation of α4β1-integrins or β2-integrins in monocytic cells (Fig. 6E, 6F). Taken together, these results suggest that Slit2 does not affect early steps involved in monocyte recruitment: monocyte capture by activated endothelium, rolling on endothelium, or activation of monocyte α4β1- and β2-integrins.

Slit2 inhibits monocyte adhesion stabilization under shear flow

Although we did not observe any effect of Slit2 on monocyte rolling and tethering to endothelium in a flow chamber under low shear conditions, Slit2 inhibited adhesion of monocytic cells to endothelial cells in static adhesion assays (Fig. 4). In these experiments, nonadherent monocytic cells are removed by centrifugation, which effectively exposes cells to higher detachment forces (36). Therefore, we questioned whether Slit2 may affect dynamic stabilization of firm monocyte adhesion, an actin-dependent and Rac1-dependent process that strengthens integrin anchors to the cortical cytoskeleton of the cell (11). To test this idea, detachment

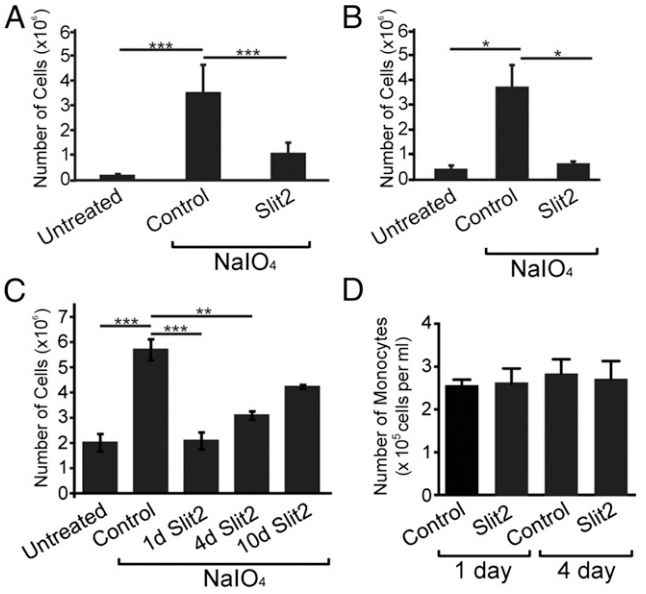

FIGURE 5. Slit2 inhibits monocyte/macrophage recruitment in vivo. (**A**) BALB/cJ mice were injected i.p. with Slit2 (2 μg) or control vehicle and 1 h later with 1 ml sodium periodate ($NaIO_4$; 5 mM). After 24 h, peritoneal exudate was collected by lavage with chilled PBS (5 ml/mouse). The number of infiltrating macrophages was quantified. Data are mean ± SEM from five separate experiments. (**B**) CD1 mice received Slit2 (2 μg) i.v. by tail vein injection, and peritonitis experiments were performed as in (A). Data are mean ± SEM from four separate experiments. (**C**) Experiments were performed as in (B) after administering Slit2 1, 4, or 10 d prior to induction of peritonitis. Data are mean ± SEM from six separate experiments. (**D**) CD1 mice received control vehicle or Slit2 (2 μg) i.p. After 24 h, blood was collected by cardiac puncture and labeled with anti-Ly6C allophycocyanin Ab, biotin anti-CD115 Ab, and streptavidin–Alexa Fluor 488. The number of $Ly6C^+/CD115^+$ monocytes was assessed by flow cytometry. Data are mean ± SEM from 10 animals. $*p < 0.05$, $**p < 0.01$, $***p < 0.001$.

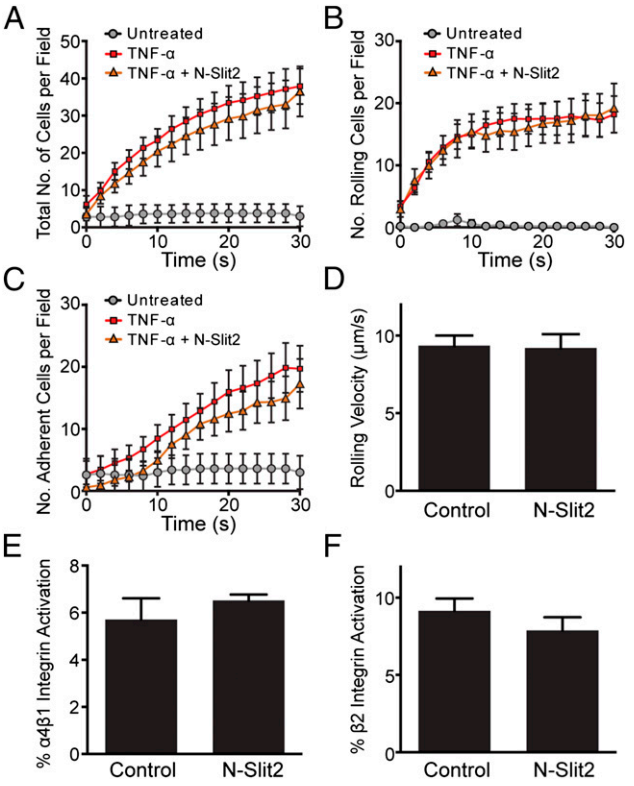

FIGURE 6. Slit2 does not affect monocyte capture, accumulation, rolling velocity, or affinity upregulation of integrins. HUVEC grown to confluence in channels of the BioFlux microfluidic system were incubated with TNF-α for 4 h. Calcein, AM-labeled U937 cells were preincubated with PBS or N-Slit2 (30 nM) and then perfused through the channels at a shear rate of 2 dyn/cm^2. A Nikon TE2000 inverted microscope and Hamamatsu video camera were used to record U937 cell–HUVEC interactions. U937 cell adhesion was quantified using ImageJ software. (**A**) Interactions between U937 cells and endothelial cells were recorded after 20 s of flow at 2 dyn/cm^2, and the total number of monocytic cells interacting with the endothelium (rolling and adherent) was quantified. Data are mean ± SEM from five separate experiments. (**B**) Experiments were performed as in (A), and the number of rolling monocytic cells was quantified. Data are mean ± SEM from five separate experiments. (**C**) Experiments were performed as in (A), and the number of firmly adherent cells was quantified (defined as cells that did not move for a 2-s interval). Data are mean ± SEM from five separate experiments. (**D**) Experiments were performed as in (A), and the rolling velocity was calculated. Data are mean ± SEM from five separate experiments. (**E**) U937 cells were pretreated with control vehicle or N-Slit2 (30 nM) and stimulated with Mn^{2+} or CXCL12 (100 ng/ml) for 2 min. FITC-conjugated peptide 4-((N′-2-methylphenyl)ureido)-phenylacetyl-*l*-leucyl-*l*-α-aspartyl-*l*-valyl- *l*-prolyl-*l*-alanyl-*l*-alanyl-*l*-lysine binding was analyzed by flow cytometry. Data are mean ± SEM from five separate experiments. (**F**) U937 cells were pretreated with control vehicle or N-Slit2 (30 nM) and stimulated with Mn^{2+} or CXCL12 in the presence of the CD11α activation epitope reporter mAb 24, labeled with FITC-conjugated secondary Ab on ice, and analyzed by flow cytometry. Data are mean ± SEM from seven separate experiments.

assays were performed in which monocytic cells were allowed to adhere to activated endothelial cells and then were exposed to increasing shear forces of up to 20 dyn/cm^2 (11). Monocytic cells readily detached from endothelial monolayers under basal conditions, and <20% of monocytic cells stabilized their adhesions at shear forces > 4 dyn/cm^2 (Fig. 7A). Activation of endothelial monolayers with TNF-α significantly increased the number of monocytic cells that resisted detachment (Fig. 7A, $p < 0.001$ for ≥1 dyn/cm^2). At all shear forces ≥ 3 dyn/cm^2, N-Slit2 exposure caused monocytic cells to detach more readily (Fig. 7A, $p < 0.01$). Exposure to LatB, an inhibitor of actin polymerization, similarly inhibited adhesion stabilization of monocytes (Fig. 7A, $p < 0.001$ for ≥ 2 dyn/cm^2). These results suggest that dynamic actin polymerization is required for adhesion stabilization and that Slit2 interferes with this process.

To determine whether Slit2 prevents adhesion stabilization of monocytes on endothelial cells by binding Robo-1, we incubated a soluble decoy of the Robo-1 receptor RoboN with N-Slit2 prior to incubation with monocytic cells. Under basal conditions, monocytic cells readily detached from endothelial monolayers (Fig. 7B). Activation of endothelial monolayers with TNF-α significantly increased the number of cells that resisted detachment (Fig. 7B, $p < 0.001$ for ≥ 1 dyn/cm^2). Above 4 dyn/cm^2, N-Slit2 exposure caused monocytes to detach more readily (Fig. 7B, $p < 0.05$, N-Slit2 versus control at 4 dyn/cm^2; $p < 0.01$, N-Slit2 versus control at 5-7 dyn/cm^2; $p < 0.001$, N-Slit2 versus control at 8-20 dyn/cm^2). RoboN had no effect, but when RoboN was added to N-Slit2 prior to incubation with cells, significantly less detachment of monocytes was observed compared with N-Slit2 alone (Fig. 7B, $p < 0.01$ for 8-20 dyn/cm^2; $p < 0.05$ for 5-7 dyn/cm^2). These results suggest that the effect of Slit2 on adhesion stabilization of monocytes is specifically mediated by Robo-1.

Slit2 inhibits adhesion stabilization of monocytic cells by preventing activation of Rac1

To determine whether Slit2 prevents adhesion stabilization of monocytes on endothelial cells by preventing activation of Rac1, we expressed CA-Rac1-GFP in monocytic cells. CA-Rac1-GFP is

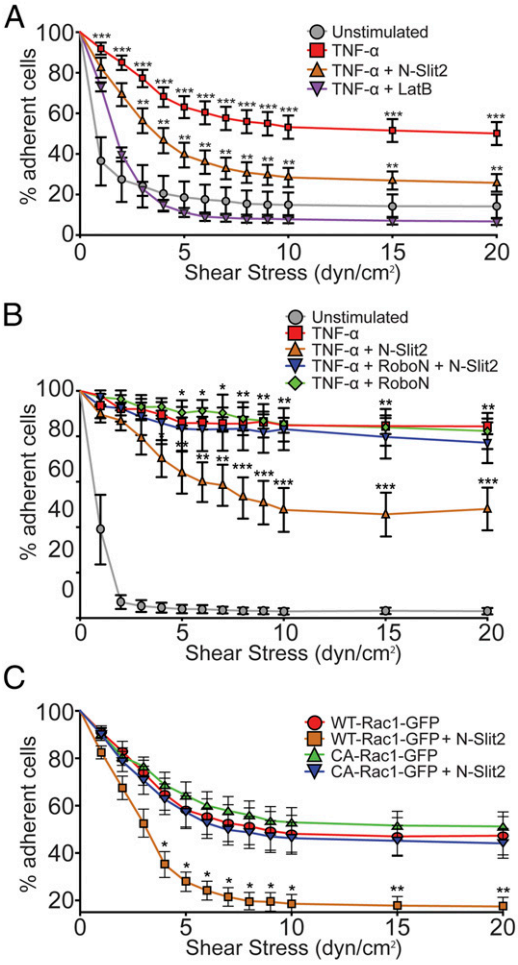

FIGURE 7. Slit2 inhibits stabilization of adhesive contacts of monocytic cells tethered to endothelial cells. (**A**) HUVEC monolayers were incubated with TNF-α for 4 h in a BioFlux microfluidic chamber. U937 cells were incubated with N-Slit2 (30 nM, 10 min) or LatB (2 μM, 5 min) before infusing them at 2 dyn/cm^2 and allowing them to settle for 1 min. Shear stress was gradually increased by 1 dyn/cm^2 every 10 s up to 20 dyn/cm^2. The number of adherent cells was expressed as a percentage of the initial cells in the channel. Data are mean ± SEM from seven independent experiments. ***$p < 0.001$, unstimulated versus TNF-α, **$p < 0.01$, TNF-α versus N-Slit2. (**B**) U937 cells were incubated with N-Slit2 (30 nM) and/or RoboN (60 nM), and experiments were performed as in (A). Data are mean ± SEM from seven independent experiments. *$p < 0.05$, TNF-α versus N-Slit2 at 4 dyn/cm^2, N-Slit2 versus N-Slit2 + Robo-N at 5–7 dyn/cm^2, ***$p < 0.001$, TNF-α versus N-Slit2 at ≥ 8 dyn/cm^2, **$p < 0.01$, TNF-α versus N-Slit2 at 5–7 dyn/cm^2, N-Slit2 versus N-Slit2 + RoboN at ≥8 dyn/cm^2. (**C**) U937 cells were electroporated with WT-Rac1-GFP or CA-Rac1-GFP and labeled with DAPI to exclude dead cells, and live GFP$^+$ cells were isolated by FACS using an Astrios MoFlo flow cytometer. WT-Rac1-GFP– or CA-Rac1-GFP–expressing cells were incubated with N-Slit2 or control vehicle, and experiments were performed as in (A). Data are mean ± SEM from 11 independent experiments. *$p < 0.05$, WT-Rac1-GFP and N-Slit2 versus WT-Rac1-GFP at 4–10 dyn/cm^2, **$p < 0.01$, WT-Rac1-GFP and N-Slit2 versus WT-Rac1-GFP at 15–20 dyn/cm^2.

unable to hydrolyze GTP and, thus, cannot be inactivated (22). Monocytic cells expressing WT-Rac1-GFP readily stabilized their adhesions to TNF-α–activated endothelial monolayers, and N-Slit2 caused these cells to detach more readily (Fig. 7C, $p < 0.05$ for 4–10 dyn/cm^2; $p < 0.01$ for 15 and 20 dyn/cm^2). Cells expressing CA-Rac1-GFP demonstrated strong adhesion stabilization, even in the presence of N-Slit2 (Fig. 7C). Collectively, these data demonstrate that Slit2 inhibits postadhesion stabilization of

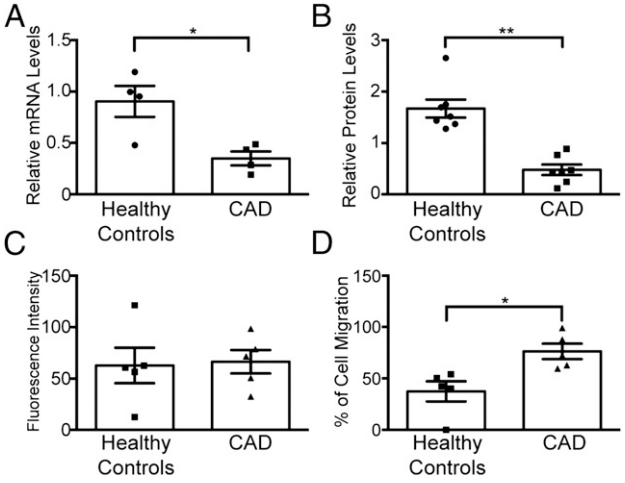

FIGURE 8. PBMC from patients with CAD display reduced levels of Robo-1 and decreased response to the actions of Slit2. (**A**) PBMC were isolated from patients with CAD and from age- and sex-matched control subjects. RNA was extracted, and RT-PCR was performed using Robo-1–specific primers. Data are mean ± SEM from four 4 patients with CAD and four healthy control subjects. (**B**) PBMC were isolated as in (A), and protein was extracted. Immunoblotting was performed using anti–Robo-1 Ab. Blots were stripped and reprobed with anti–β-actin Ab, and levels of Robo-1 were normalized to β-actin using the VersaDoc Imaging System (Bio-Rad). Data are mean ± SEM from seven patients with CAD and seven control subjects. (**C**) PBMC were isolated as in (A), and chemotaxis assays were performed as in Fig. 2, examining PBMC migration toward CCL2 (50 ng/ml). Data are mean ± SEM from five patients with CAD and five control subjects. (**D**) PBMC were incubated with Slit2 (10 nM) for 10 min, and chemotaxis experiments were performed. Percentage of PBMC migration toward CCL2 in the presence of Slit2 in CAD patients and healthy controls. Data are mean ± SEM from five patients with CAD and five healthy control subjects. *$p < 0.05$, **$p < 0.01$.

monocytic cells tethered to endothelial cells by preventing activation of Rac1.

PBMC from patients with CAD have decreased levels of Robo-1 and show decreased response to the actions of Slit2

Our results showed that by binding to leukocyte-expressed Robo-1, Slit2 prevented adhesion stabilization of monocytes on endothelial cells and, thus, could potentially temper leukocyte influx associated with vascular inflammation. Therefore, we determined whether levels of Robo-1 in leukocytes are altered in patients with cardiovascular disease. Accordingly, we found that PBMC from patients with CAD displayed significantly less Robo-1 mRNA and protein than did PBMC from healthy, matched control subjects (Fig. 8A, 8B, mRNA, $p < 0.05$; protein, $p < 0.01$). We next determined whether PBMC from patients with CAD are indeed less responsive to the actions of Slit2. PBMC from patients with CAD and from healthy individuals demonstrated similar chemotaxis toward CCL2 (Fig. 8C). However, the ability of Slit2 to inhibit cell migration was significantly dampened in PBMC from patients with CAD (Fig. 8D, $p < 0.05$). Together, these data suggest that low levels of Robo-1 in PBMC from patients with CAD may be a risk factor that could prevent Slit2-mediated inhibition of leukocyte recruitment in early vascular inflammation.

Slit2 inhibits early trafficking of monocytes into nascent atherosclerotic lesions

To directly test whether Slit2 can inhibit early monocyte recruitment into nascent atherosclerotic lesions, we used BrdU pulse labeling combined with en face confocal microscopy to assess

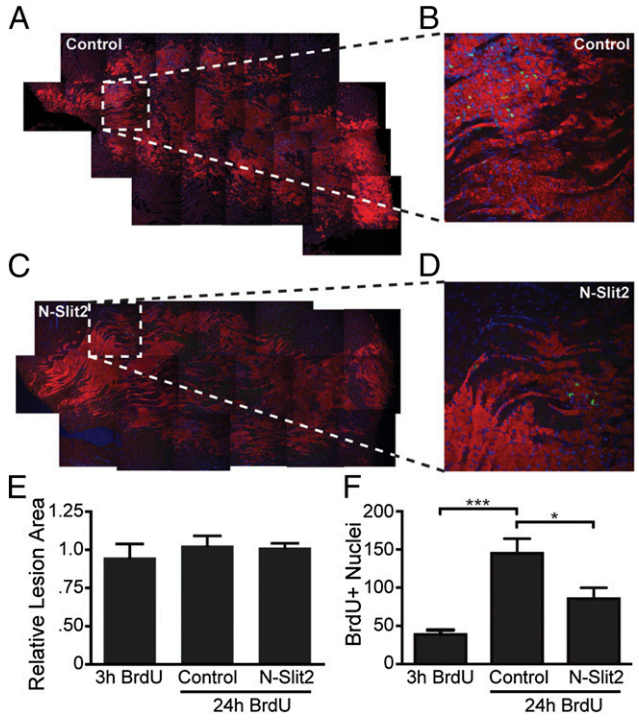

FIGURE 9. Slit2 inhibits monocyte recruitment to nascent atherosclerotic lesions. (**A**) *Ldlr*$^{-/-}$ mice were fed a cholesterol-rich diet for 3 wk and pulsed with BrdU for 24 h, and control vehicle was administered i.v. After 24 h, aortas were removed and labeled with Nile Red and CD45 (data not shown). Composite of en face images taken with a 40× objective shows the entire Nile Red–labeled lesion area (red) in the lower curvature of the ascending aortic arch (FV-1000; Olympus). (**B**) High-power images (original magnification ×40) of the regions in (A) indicated by dashed lines. BrdU$^+$ nuclei (green) and intimal lipid accumulation (red) were visualized. (**C**) Experiments were performed as in (A), but mice were given N-Slit2 (5 μg) i.v. instead of control vehicle. (**D**) High-power images (original magnification ×40) of the regions in (C) indicated by dashed lines. (**E**) Experiments were performed as in (A) and (C). Lesion areas relative to the value for the control group were determined using ImageJ software. (**F**) Experiments were performed as in (A) and (C). Intimal BrdU$^+$ nuclei were enumerated at 3 and 24 h after BrdU pulse labeling. The entire surface of the ascending aorta above the aortic valve was scanned by en face confocal microscopy. For each condition, at least three independent experiments were performed. Data are mean ± SEM derived from four to seven mice. $^*p < 0.05$, $^{***}p < 0.001$.

recruitment of Ly6C^{high} monocytes to 3-wk lesions in *Ldlr*$^{-/-}$ mice (28, 37). As expected, a single injection of N-Slit2 21 h before analysis did not influence the extent of lipid accumulation in lesions, as determined by Nile Red staining (Fig. 9A, 9C, 9E). However, N-Slit2 significantly reduced the number of BrdU-labeled nuclei in CD45$^+$ cells 24 h after BrdU injection (145 ± 19 versus 86 ± 14, $p < 0.05$, Fig. 9B, 9D, 9F). The number of proliferating macrophages in lesions was the same for both groups, and is indicated by BrdU$^+$ nuclei 3 h after injection (Fig. 9F). Together, these data suggest that Slit2 inhibits influx of monocytes into early vascular lesions.

Discussion

We report in this article that human and mouse monocytes express the Slit2 receptor Robo-1 and that Slit2 blocks monocyte migration toward different chemotactic gradients by inhibiting activation of Rac1 and Cdc42, as well as Akt and Erk. Our findings are in keeping with those of Geutskens et al. (38), who reported that human monocytes express Robo-1, but not Robo-2 or Robo-3, as well as with signaling studies performed in neutrophils, vascular smooth muscle cells, T lymphocytes, breast cancer cells, and neuronal cells (14–17, 20). Moreover, Prasad et al. (16) showed that monocytes express Robo-1 and that Slit2 blocks chemotaxis toward CXCL12. We extend these findings to show that Slit2 also blocks chemotaxis of monocytes toward a chemokine of a different class: CCL2. Although our study did not distinguish between directional chemotaxis and random chemokinesis, we demonstrated previously that, in human neutrophils, Slit2 blocked directional chemotaxis and not random chemokinesis (17).

In vascular inflammation, the local cytokine microenvironment activates endothelial cells to express increased levels of adhesion molecules, notably ICAM-1 and VCAM-1, in turn facilitating efficient capture of circulating monocytes, their firm arrest, and diapedesis across the vessel wall. We found that Slit2 inhibited adhesion of monocytes to activated endothelial cells. Our observations are consistent with work showing that Slit2 inhibited CXCL12-mediated adhesion of human breast cancer cells to fibronectin and collagen (15). Recently, Zhao et al. (39) demonstrated that Slit2 prevented adhesion of monocytic cells to activated HUVEC by inhibiting LPS-induced upregulation of ICAM-1 in endothelial cells. It is possible that Slit2 similarly inhibits upregulation of ICAM-1 on the surface of endothelial cells exposed to TNF-α, contributing to the decreased adhesion of monocytic cells that we observed. Our results suggest that Slit2 also acts directly on monocytes, because it inhibited their adhesion to immobilized ICAM-1 and VCAM-1, even in the absence of HUVEC. Furthermore, we reported previously that Slit2 inhibited static adhesion of neutrophils to TNF-α–activated HUVEC through its selective actions on neutrophils (23) and that administration of Slit2 also inhibited neutrophil recruitment into the peritoneal cavity following induction of peritonitis (17). Further exploration regarding the molecular mechanisms by which Slit2 differentially affects endothelial cells following exposure to varied inflammatory stimuli is needed.

Because the Rho family GTPases, Rac1 and Cdc42, also regulate the actin rearrangement required for monocyte adhesion (11, 40), signaling events downstream of Slit2/Robo-1 could influence the ability of monocytes to form and maintain adhesive contacts. G protein–coupled receptor engagement by chemokines during monocyte rolling induces outside-in signaling, which increases integrin avidity on monocytes (25). We did not observe any effect of Slit2 on transient upregulation of monocyte integrin affinity induced by CXCL12. Because cytoskeletal regulation couples conformational changes of LFA-1 to lateral mobility and clustering of the receptor, it is possible that Slit2 affects the overall avidity of monocyte integrins via cytoskeletal changes (41). Although Slit2 had no effect on monocyte integrin affinity or on tethering and capture of monocytes exposed to shear flow, it significantly inhibited adhesion stabilization of monocytes bound to endothelial cells in a Robo-1– and Rac1-dependent manner. These results are consistent with the previous demonstration that Rac1 mediates the dynamic actin polymerization required for stabilization of adhesive contacts of monocytes bound to endothelial cells (11). Importantly, the shear forces used in our study are similar to those that would be encountered by monocytes tethered to vascular endothelium in early atherosclerotic lesions (42).

We noted reduced levels of Robo-1 in PBMC from patients with CAD compared with matched control subjects, but the mechanisms underlying these differences are unknown. A recent study demonstrated that Robo-1 expression is downregulated in endothelial cells via targeting of miR-218 (39). Because Robo-1 is a single-pass transmembrane protein, cell surface levels could, in principle, also be determined by endocytosis and recycling back to the plasma membrane. In addition, plasmalemmal Robo-1 was

shown to undergo sequential proteolysis by metalloproteases and γ-secretase, resulting in proteolytic release of the Robo-1 ectodomain and accumulation within the nucleus of the C-terminal fragment of the protein (43–45). Although beyond the scope of our present study, a detailed exploration of how the proinflammatory milieu seen in vascular inflammation and atherosclerosis influences regulation of Robo-1 in leukocytes would be of great clinical and translational interest.

Early influx of monocytes into affected vessels plays a critical role in shaping the subsequent development of atherosclerotic lesions (5, 6). We found that Slit2 blocked monocyte chemotaxis to different classes of chemokines, as well as inhibited adhesion stabilization of monocytes tethered to endothelial cells. We (17) and other investigators (18) demonstrated that Slit2 prevents chemotaxis of leukocytes toward chemokines, as well as other chemoattractants. Thus, by simultaneously targeting varied chemotactic signals, Slit2 could potently inhibit monocyte recruitment to injured vessels. Accordingly, we noted that administration of Slit2 attenuated monocyte recruitment to nascent atherosclerotic lesions.

Atherogenesis involves a complex, interconnected series of events, including monocyte infiltration, as well as recruitment of neutrophils and T lymphocytes, VSMC migration from the medial to the intimal layer of the vessel, and platelet adhesion to the injured vessel wall (1, 2, 46). Slit2 can inhibit each of these processes. Slit2 was shown to inhibit chemotaxis of neutrophils and T lymphocytes to various chemoattractants, including fMLF and chemokines (16, 17). Slit2 was also noted to inhibit VSMC migration toward platelet-derived growth factor (14). We reported that Slit2 is a potent inhibitor of platelet function both in vitro and in vivo and that it prevents thrombosis in injured arteries and arterioles (21). Thus, Slit2 could represent an exciting therapeutic candidate to simultaneously inhibit the individual events that collectively promote the initiation and progression of vascular inflammation associated with atherosclerosis. Other guidance cues, such as ephrin B2, netrin1, and semaphorin 3E, are differentially regulated in proatherogenic conditions; however, overall, these factors appear to exacerbate, and not attenuate, progressive vascular injury (47–49). Further studies are needed to determine whether Slit2 is unique among these cues, preventing early trafficking of monocytes into affected vessels, as we report in this article, as well as advanced lesion progression.

Acknowledgments

We thank Dr. Sergio Grinstein for critical feedback and reagents. We are grateful to Annie Bang for assistance with flow cytometry.

Disclosures

The authors have no financial conflicts of interest.

References

1. Meadows, T. A., and D. L. Bhatt. 2007. Clinical aspects of platelet inhibitors and thrombus formation. *Circ. Res.* 100: 1261–1275.
2. Libby, P. 2002. Inflammation in atherosclerosis. *Nature* 420: 868–874.
3. Ortlepp, J. R., K. Vesper, V. Mevissen, F. Schmitz, U. Janssens, A. Franke, P. Hanrath, C. Weber, K. Zerres, and R. Hoffmann. 2003. Chemokine receptor (CCR2) genotype is associated with myocardial infarction and heart failure in patients under 65 years of age. *J. Mol. Med.* 81: 363–367.
4. McDermott, D. H., J. P. Halcox, W. H. Schenke, M. A. Waclawiw, M. N. Merrell, N. Epstein, A. A. Quyyumi, and P. M. Murphy. 2001. Association between polymorphism in the chemokine receptor CX3CR1 and coronary vascular endothelial dysfunction and atherosclerosis. *Circ. Res.* 89: 401–407.
5. Combadière, C., S. Potteaux, M. Rodero, T. Simon, A. Pezard, B. Esposito, R. Merval, A. Proudfoot, A. Tedgui, and Z. Mallat. 2008. Combined inhibition of CCL2, CX3CR1, and CCR5 abrogates Ly6C(hi) and Ly6C(lo) monocytosis and almost abolishes atherosclerosis in hypercholesterolemic mice. *Circulation* 117: 1649–1657.
6. Saederup, N., L. Chan, S. A. Lira, and I. F. Charo. 2008. Fractalkine deficiency markedly reduces macrophage accumulation and atherosclerotic lesion formation in CCR2$^{-/-}$ mice: evidence for independent chemokine functions in atherogenesis. *Circulation* 117: 1642–1648.
7. Boring, L., J. Gosling, S. W. Chensue, S. L. Kunkel, R. V. Farese, Jr., H. E. Broxmeyer, and I. F. Charo. 1997. Impaired monocyte migration and reduced type 1 (Th1) cytokine responses in C-C chemokine receptor 2 knockout mice. *J. Clin. Invest.* 100: 2552–2561.
8. Gosling, J., S. Slaymaker, L. Gu, S. Tseng, C. H. Zlot, S. G. Young, B. J. Rollins, and I. F. Charo. 1999. MCP-1 deficiency reduces susceptibility to atherosclerosis in mice that overexpress human apolipoprotein B. *J. Clin. Invest.* 103: 773–778.
9. Lesnik, P., C. A. Haskell, and I. F. Charo. 2003. Decreased atherosclerosis in CX3CR1$^{-/-}$ mice reveals a role for fractalkine in atherogenesis. *J. Clin. Invest.* 111: 333–340.
10. Swirski, F. K., M. J. Pittet, M. F. Kircher, E. Aikawa, F. A. Jaffer, P. Libby, and R. Weissleder. 2006. Monocyte accumulation in mouse atherogenesis is progressive and proportional to extent of disease. *Proc. Natl. Acad. Sci. USA* 103: 10340–10345.
11. Rullo, J., H. Becker, S. J. Hyduk, J. C. Wong, G. Digby, P. D. Arora, A. P. Cano, J. Hartwig, C. A. McCulloch, and M. I. Cybulsky. 2012. Actin polymerization stabilizes α4β1 integrin anchors that mediate monocyte adhesion. *J. Cell Biol.* 197: 115–129.
12. Brose, K., K. S. Bland, K. H. Wang, D. Arnott, W. Henzel, C. S. Goodman, M. Tessier-Lavigne, and T. Kidd. 1999. Slit proteins bind Robo receptors and have an evolutionarily conserved role in repulsive axon guidance. *Cell* 96: 795–806.
13. Kidd, T., K. S. Bland, and C. S. Goodman. 1999. Slit is the midline repellent for the robo receptor in *Drosophila*. *Cell* 96: 785–794.
14. Liu, D., J. Hou, X. Hu, X. Wang, Y. Xiao, Y. Mou, and H. De Leon. 2006. Neuronal chemorepellent Slit2 inhibits vascular smooth muscle cell migration by suppressing small GTPase Rac1 activation. *Circ. Res.* 98: 480–489.
15. Prasad, A., A. Z. Fernandis, Y. Rao, and R. K. Ganju. 2004. Slit protein-mediated inhibition of CXCR4-induced chemotactic and chemoinvasive signaling pathways in breast cancer cells. *J. Biol. Chem.* 279: 9115–9124.
16. Prasad, A., Z. Qamri, J. Wu, and R. K. Ganju. 2007. Slit-2/Robo-1 modulates the CXCL12/CXCR4-induced chemotaxis of T cells. *J. Leukoc. Biol.* 82: 465–476.
17. Tole, S., I. M. Mukovozov, Y. W. Huang, M. A. Magalhaes, M. Yan, M. R. Crow, G. Y. Liu, C. X. Sun, Y. Durocher, M. Glogauer, and L. A. Robinson. 2009. The axonal repellent, Slit2, inhibits directional migration of circulating neutrophils. *J. Leukoc. Biol.* 86: 1403–1415.
18. Wu, J. Y., L. Feng, H. T. Park, N. Havlioglu, L. Wen, H. Tang, K. B. Bacon, Jiang Zh, Zhang Xc, and Y. Rao. 2001. The neuronal repellent Slit inhibits leukocyte chemotaxis induced by chemotactic factors. *Nature* 410: 948–952.
19. Kanellis, J., G. E. Garcia, P. Li, G. Parra, C. B. Wilson, Y. Rao, S. Han, C. W. Smith, R. J. Johnson, J. Y. Wu, and L. Feng. 2004. Modulation of inflammation by slit protein in vivo in experimental crescentic glomerulonephritis. *Am. J. Pathol.* 165: 341–352.
20. Wong, K., X. R. Ren, Y. Z. Huang, Y. Xie, G. Liu, H. Saito, H. Tang, L. Wen, S. M. Brady-Kalnay, L. Mei, et al. 2001. Signal transduction in neuronal migration: roles of GTPase activating proteins and the small GTPase Cdc42 in the Slit-Robo pathway. *Cell* 107: 209–221.
21. Patel, S., Y. W. Huang, A. Reheman, F. G. Pluthero, S. Chaturvedi, I. M. Mukovozov, S. Tole, G. Y. Liu, L. Li, Y. Durocher, et al. 2012. The cell motility modulator Slit2 is a potent inhibitor of platelet function. *Circulation* 126: 1385–1395.
22. Yeung, T., G. E. Gilbert, J. Shi, J. Silvius, A. Kapus, and S. Grinstein. 2008. Membrane phosphatidylserine regulates surface charge and protein localization. *Science* 319: 210–213.
23. Chaturvedi, S., D. A. Yuen, A. Bajwa, Y. W. Huang, C. Sokollik, L. Huang, G. Y. Lam, S. Tole, G. Y. Liu, J. Pan, et al. 2013. Slit2 prevents neutrophil recruitment and renal ischemia-reperfusion injury. *J. Am. Soc. Nephrol.* 24: 1274–1287.
24. Morlot, C., N. M. Thielens, R. B. Ravelli, W. Hemrika, R. A. Romijn, P. Gros, S. Cusack, and A. A. McCarthy. 2007. Structural insights into the Slit-Robo complex. *Proc. Natl. Acad. Sci. USA* 104: 14923–14928.
25. Chan, J. R., S. J. Hyduk, and M. I. Cybulsky. 2001. Chemoattractants induce a rapid and transient upregulation of monocyte alpha4 integrin affinity for vascular cell adhesion molecule 1 which mediates arrest: an early step in the process of emigration. *J. Exp. Med.* 193: 1149–1158.
26. Jiang, N., and D. S. Pisetsky. 2005. The effect of inflammation on the generation of plasma DNA from dead and dying cells in the peritoneum. *J. Leukoc. Biol.* 77: 296–302.
27. Dransfield, I., C. Cabañas, J. Barrett, and N. Hogg. 1992. Interaction of leukocyte integrins with ligand is necessary but not sufficient for function. *J. Cell Biol.* 116: 1527–1535.
28. Lichtman, A. H., S. K. Clinton, K. Iiyama, P. W. Connelly, P. Libby, and M. I. Cybulsky. 1999. Hyperlipidemia and atherosclerotic lesion development in LDL receptor-deficient mice fed defined semipurified diets with and without cholate. *Arterioscler. Thromb. Vasc. Biol.* 19: 1938–1944.
29. Zhu, S. N., M. Chen, J. Jongstra-Bilen, and M. I. Cybulsky. 2009. GM-CSF regulates intimal cell proliferation in nascent atherosclerotic lesions. *J. Exp. Med.* 206: 2141–2149.
30. Weber, C., R. Alon, B. Moser, and T. A. Springer. 1996. Sequential regulation of alpha 4 beta 1 and alpha 5 beta 1 integrin avidity by CC chemokines in monocytes: implications for transendothelial chemotaxis. *J. Cell Biol.* 134: 1063–1073.

31. Anand, A. R., H. Zhao, T. Nagaraja, L. A. Robinson, and R. K. Ganju. 2013. N-terminal Slit2 inhibits HIV-1 replication by regulating the actin cytoskeleton. *Retrovirology* 10: 2.
32. Arai, A., M. Aoki, Y. Weihua, A. Jin, and O. Miura. 2006. CrkL plays a role in SDF-1-induced activation of the Raf-1/MEK/Erk pathway through Ras and Rac to mediate chemotactic signaling in hematopoietic cells. *Cell. Signal.* 18: 2162–2171.
33. Nishiya, N., W. B. Kiosses, J. Han, and M. H. Ginsberg. 2005. An alpha4 integrin-paxillin-Arf-GAP complex restricts Rac activation to the leading edge of migrating cells. *Nat. Cell Biol.* 7: 343–352.
34. van Helden, S. F., E. C. Anthony, R. Dee, and P. L. Hordijk. 2012. Rho GTPase expression in human myeloid cells. *PLoS One* 7: e42563.
35. Gerszten, R. E., E. B. Friedrich, T. Matsui, R. R. Hung, L. Li, T. Force, and A. Rosenzweig. 2001. Role of phosphoinositide 3-kinase in monocyte recruitment under flow conditions. *J. Biol. Chem.* 276: 26846–26851.
36. Reyes, C. D., and A. J. García. 2003. A centrifugation cell adhesion assay for high-throughput screening of biomaterial surfaces. *J. Biomed. Mater. Res. A* 67: 328–333.
37. Ishibashi, S., J. L. Goldstein, M. S. Brown, J. Herz, and D. K. Burns. 1994. Massive xanthomatosis and atherosclerosis in cholesterol-fed low density lipoprotein receptor-negative mice. *J. Clin. Invest.* 93: 1885–1893.
38. Geutskens, S. B., P. L. Hordijk, and P. B. van Hennik. 2010. The chemorepellent Slit3 promotes monocyte migration. *J. Immunol.* 185: 7691–7698.
39. Zhao, H., A. R. Anand, and R. K. Ganju. 2014. Slit2-Robo4 pathway modulates lipopolysaccharide-induced endothelial inflammation and its expression is dysregulated during endotoxemia. *J. Immunol.* 192: 385–393.
40. Rom, S., S. Fan, N. Reichenbach, H. Dykstra, S. H. Ramirez, and Y. Persidsky. 2012. Glycogen synthase kinase 3β inhibition prevents monocyte migration across brain endothelial cells via Rac1-GTPase suppression and down-regulation of active integrin conformation. *Am. J. Pathol.* 181: 1414–1425.
41. Cairo, C. W., R. Mirchev, and D. E. Golan. 2006. Cytoskeletal regulation couples LFA-1 conformational changes to receptor lateral mobility and clustering. *Immunity* 25: 297–308.
42. Stone, P. H., A. U. Coskun, S. Kinlay, J. J. Popma, M. Sonka, A. Wahle, Y. Yeghiazarians, C. Maynard, R. E. Kuntz, and C. L. Feldman. 2007. Regions of low endothelial shear stress are the sites where coronary plaque progresses and vascular remodelling occurs in humans: an in vivo serial study. *Eur. Heart J.* 28: 705–710.
43. Ito, H., S. Funahashi, N. Yamauchi, J. Shibahara, Y. Midorikawa, S. Kawai, Y. Kinoshita, A. Watanabe, Y. Hippo, T. Ohtomo, et al. 2006. Identification of ROBO1 as a novel hepatocellular carcinoma antigen and a potential therapeutic and diagnostic target. *Clin. Cancer Res.* 12: 3257–3264.
44. Coleman, H. A., J. P. Labrador, R. K. Chance, and G. J. Bashaw. 2010. The Adam family metalloprotease Kuzbanian regulates the cleavage of the roundabout receptor to control axon repulsion at the midline. *Development* 137: 2417–2426.
45. Seki, M., A. Watanabe, S. Enomoto, T. Kawamura, H. Ito, T. Kodama, T. Hamakubo, and H. Aburatani. 2010. Human ROBO1 is cleaved by metalloproteinases and gamma-secretase and migrates to the nucleus in cancer cells. *FEBS Lett.* 584: 2909–2915.
46. Glass, C. K., and J. L. Witztum. 2001. Atherosclerosis. the road ahead. *Cell* 104: 503–516.
47. Wanschel, A., T. Seibert, B. Hewing, B. Ramkhelawon, T. D. Ray, J. M. van Gils, K. J. Rayner, J. E. Feig, E. R. O'Brien, E. A. Fisher, and K. J. Moore. 2013. Neuroimmune guidance cue Semaphorin 3E is expressed in atherosclerotic plaques and regulates macrophage retention. *Arterioscler. Thromb. Vasc. Biol.* 33: 886–893.
48. van Gils, J. M., M. C. Derby, L. R. Fernandes, B. Ramkhelawon, T. D. Ray, K. J. Rayner, S. Parathath, E. Distel, J. L. Feig, J. I. Alvarez-Leite, et al. 2012. The neuroimmune guidance cue netrin-1 promotes atherosclerosis by inhibiting the emigration of macrophages from plaques. *Nat. Immunol.* 13: 136–143.
49. van Gils, J. M., B. Ramkhelawon, L. Fernandes, M. C. Stewart, L. Guo, T. Seibert, G. B. Menezes, D. C. Cara, C. Chow, T. B. Kinane, et al. 2013. Endothelial expression of guidance cues in vessel wall homeostasis dysregulation under proatherosclerotic conditions. *Arterioscler. Thromb. Vasc. Biol.* 33: 911–919.